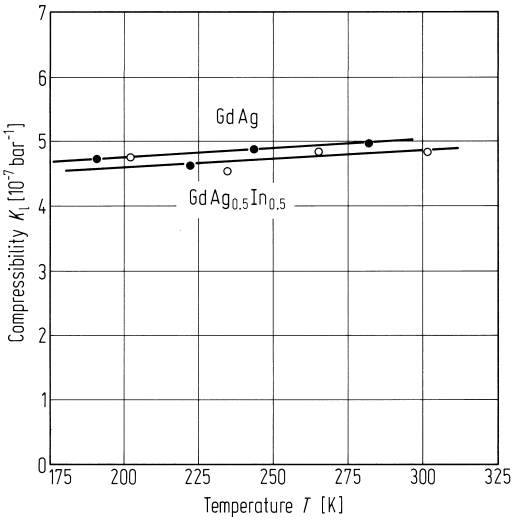

Fig. 263. Temperature dependence of the linear compressibility K_l for $GdAg_{1-x}In_x$ with x = 0 and x = 0.5 [78Y1].

Table 58. Summary of the pressure dependence of the lattice parameter, Curie and Néel temperature of $GdAg_{1-x}In_x$ compounds [78Y1].

x	a_0 [Å]	T_N [K]	T_C [K]	$\Delta T_t/\Delta p$ [10^{-4} K bar^{-1}]	$\partial \ln T_t/\partial \ln V$	K_t at 300 K [10^{-7} bar^{-1}]	$\Delta K_t/\Delta T$ [10^{-10} bar^{-1}K^{-1}]
0	3.648	139.0		0.0	0.0	5.0	3.5
0.10	3.666	131.0		0.0	0.0		
0.15	3.670	116.0		0.0	0.0		
0.20	3.681		24.0	2.5	– 7.9		
0.30	3.688		57.0	4.6	– 6.4		
0.40	3.701		92.9	7.4	– 6.0		
0.50	3.721		111.2	7.6	– 5.2	4.8	3.5

1.5.5.6 Electrical properties

Resistivity measurements have been used to investigate magnetic and structural phase transitions and to establish the onset of superconductivity. Electrical properties of superconductors are reported in subsect. 1.5.5.6.3 dealing with superconductivity.

1.5.5.6.1 Electrical resistivity

The thermal variation of $\rho(T)$ is analysed assuming a residual component ρ_0 indicating sample quality and a temperature dependent metallic contribution $\rho_m(T)$.

$$\rho(T) = \rho_0 + \rho_m(T) \tag{63}$$

A power law dependence is usually used to parameterise $\rho_m(T)$.

$$\rho_m(T) = AT^n \tag{64}$$

The exponent can indicate the type of scattering mechanism. At low temperatures, magnons in a local spin system give rise to n = 2, whereas phonons produce n = 5. An exponent n = 2 is also

expected for Fermi liquid (electron-electron) scattering and close to a magnetic transition spin disorder scattering becomes important.

X_2YZ X = 3d, Y = 3d

X = 8A: Ni
Y = 7A: Mn
Z = 3B: In; 4B: Sn; 5B: Sb

Ni_2MnZ

These materials order ferromagnetically with a moment close to 4 μ_B confined to the Mn atoms [88W1].

Table 59. A summary of the lattice parameter, residual resistivity, spontaneous magnetisation and Curie temperatures for Ni_2MnIn samples [84F1].

Sample	a_0 [10^{-1} nm]	ρ_0 [$\mu\Omega$ cm]	p_s [μ_B]	T_C [K]
1	6.072 ± 0.001	6.60 ± 0.24	4.59	321 ± 2
2	6.074 ± 0.002	6.96 ± 0.28	4.45	320 ± 2

Table 60. Ideal resistivity parameters: n, given by $\rho_i = aT^n$ and A and B, given by $\rho(T)/T = A + BT$ for Ni_2MnIn samples [84F1].

Sample	n	A [10^{-2} $\mu\Omega$ cm K^{-1}]	B [10^{-4} $\mu\Omega$ cm K^{-2}]
1	2.36 ± 0.06	1.68 ± 0.08	4.29 ± 0.21
2	2.29 ± 0.06	1.57 ± 0.08	4.43 ± 0.22

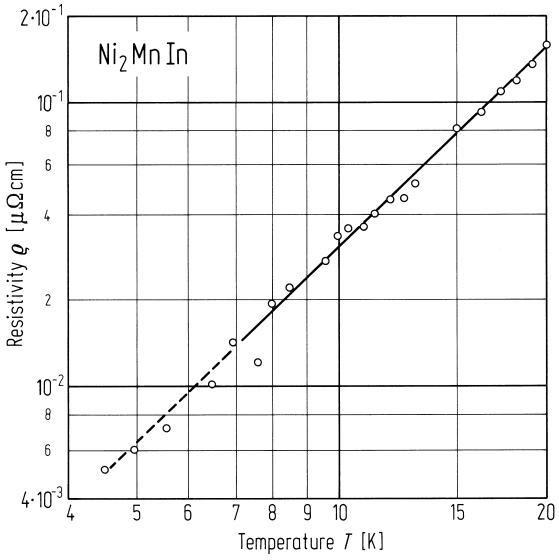

Fig. 264. Ideal resistivity (residual resistivity subtracted) as a function of temperature of Ni_2MnIn [84F1].

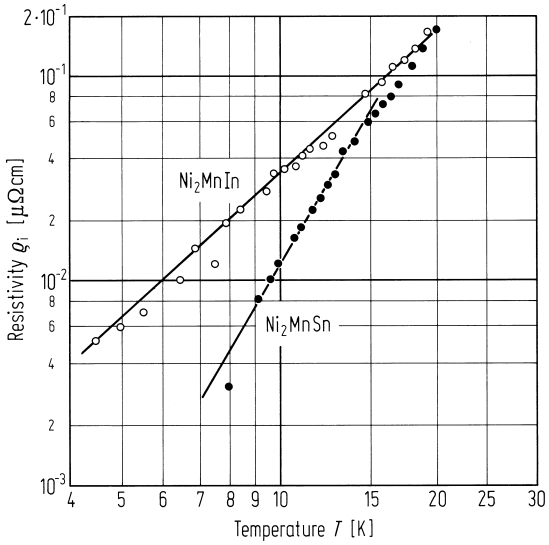

Fig. 265. Ideal electrical resistivity of Ni_2MnIn and Ni_2MnSn [91F1].

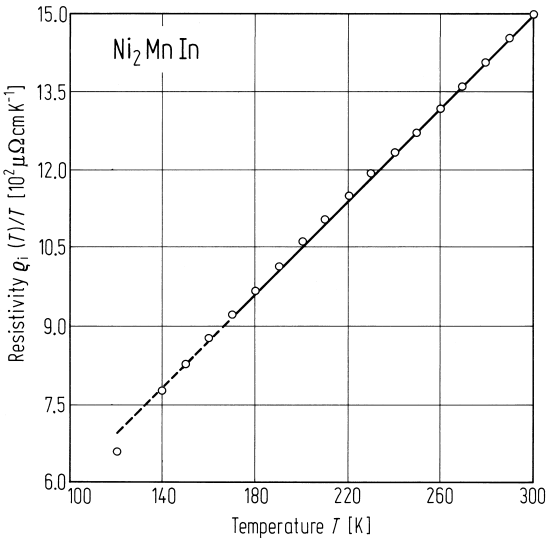

Fig. 266. Ideal electrical resistivity divided by absolute temperature, $\rho_i(T)/T$ for sample 1 defined in Table 60. The straight line is a least square fit to the values from 170 to 300 K [84F1].

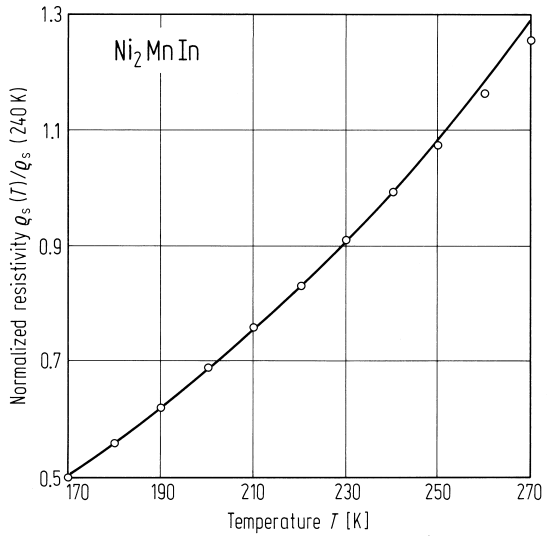

Fig. 267. Comparison of the normalised experimental magnetic contribution to the electrical resistivity ρ_s (circles) against Kasuya's [56K1] theoretical curve (solid line) for spin disorder scattering, namely

$$\rho_s(T) = C\mu^2 \frac{J_{sd}^2}{E_F}(s-\delta)(s+\delta+1).$$ [84F1].

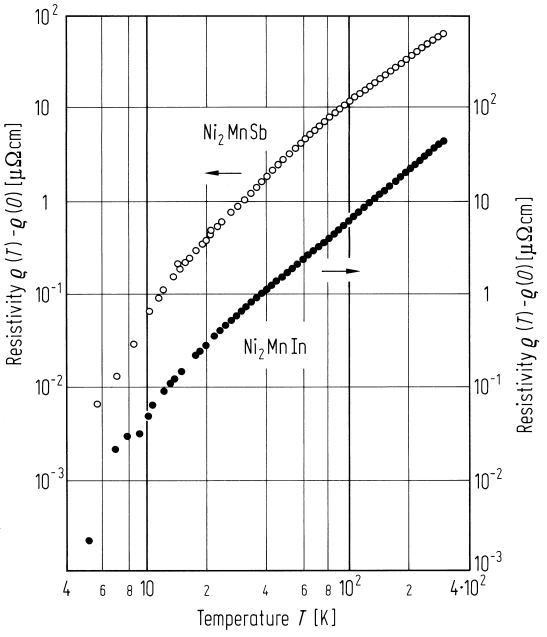

Fig. 268. Temperature dependence of the electrical resistivity of Ni_2MnSb and Ni_2MnIn [86H2].

X_2YZ X = 4d, Y = 3d

X = 8A: Pd
Y = 7A: Mn
Z = 3B: In; 4B: Sn

Pd_2MnZ

Pd_2MnIn orders antiferromagnetically with a moment of approximately 4 μ_B fixed to the Mn atoms. When ordered in the $L2_1$ structure, the Néel temperature is close to 140 K and the antiferromagnetic state is type AF2. Preferentially disordering the system into the B2 structure causes the Néel temperature to decrease. Pd_2MnSn orders ferromagnetically.

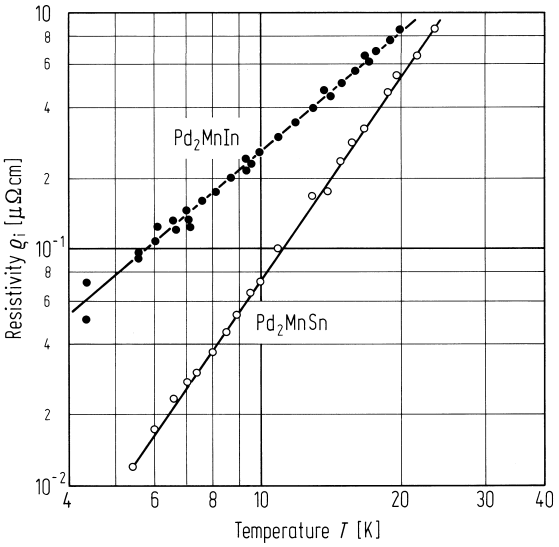

Fig. 269. Ideal electrical resistivity of Pd_2MnIn and Pd_2MnSn [91F1].

X_2YZ X = 3d, Y = 4f

X = 1B: Cu
Y = 4A: La, Ce, Sm, Nd, Pr, Yb
Z = 3B: In

Cu_2CeIn

Interest in Cu_2CeIn was primarily focused on establishing Heavy Fermion behaviour. The resistivity for both single and polycrystalline samples is similar. However, it is clear from the temperature range covered in Fig. 270 that there is not a T^2 dependence of the resistivity as expected for a Fermi liquid.

The pressure dependence has also been investigated up to 1.55 GPa, causing the resistivity maximum to increase from 23 K to 80 K.

The electrical resistivity of compounds containing La, Pr, Nd and Sm have been investigated in the temperature range 1.3 K to 300 K. The measurements undertaken on single crystals did not reveal any anomalies.

A first order valence transition $Yb^{2+} \rightarrow Yb^{3+}$ is reported at 50 K in $Yb_{0.4}In_{0.6}Cu_2$ [86F1]. An increase in the resistivity was observed at 50 K [87F1].

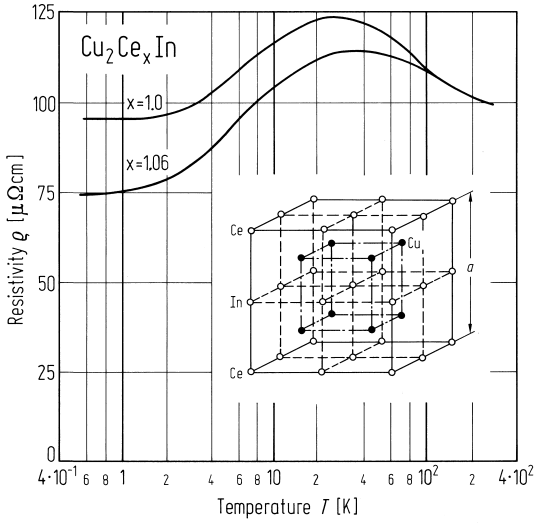

Fig. 270. Temperature dependence of electrical resistivity for a Cu_2CeIn single crystal and $Cu_2Ce_{1.06}$ In polycrystal. The inset shows the cubic Heusler structure of Cu_2CeIn [87O2].

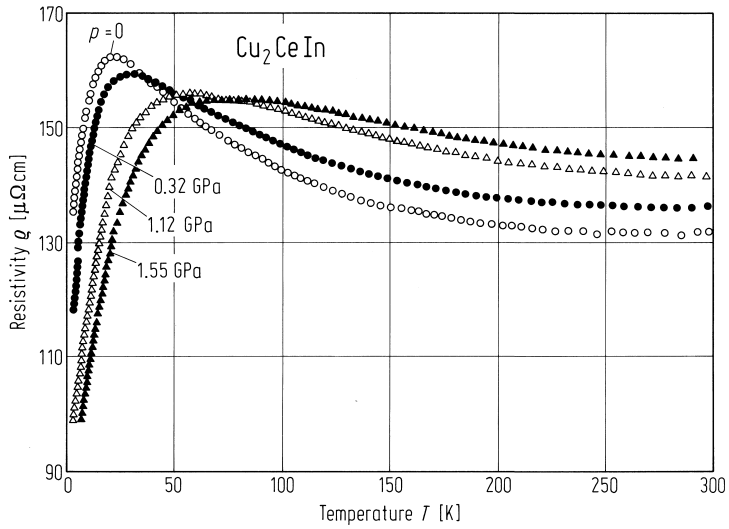

Fig. 271. Bulk electrical resistivity of Cu_2CeIn under pressure: p = 0, 0.32 GPa, 1.12 GPa and 1.55 GPa [87N1].

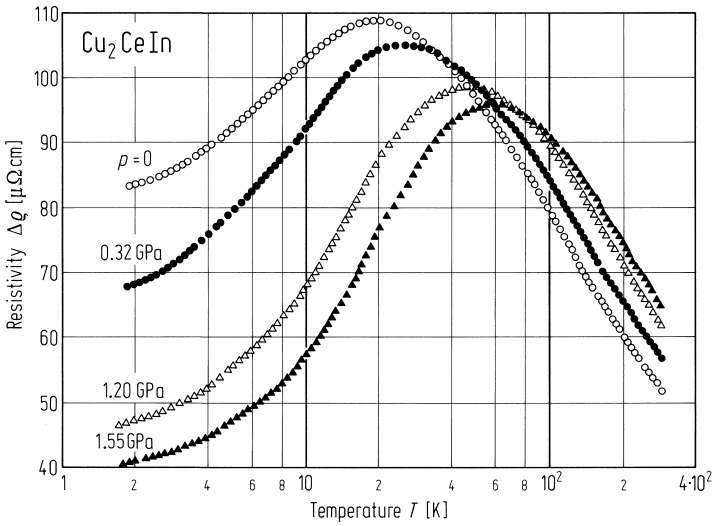

Fig. 272. Magnetic contribution to the electrical resistivity of Cu_2CeIn plotted against the decimal logarithm of the temperature at p = 0, 0.32 GPa, 1.2 GPa and 1.55 GPa [87N1].

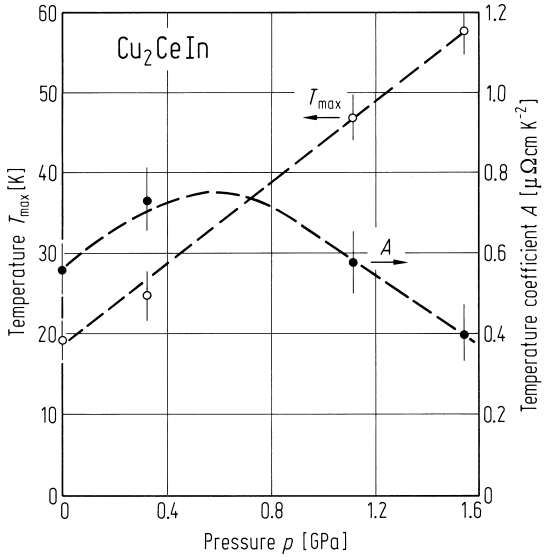

Fig. 273. Pressure dependence of T_{max} and of the coefficient of the T^2 term of the low temperature electrical resistivity, A, for Cu_2CeIn [87N1].

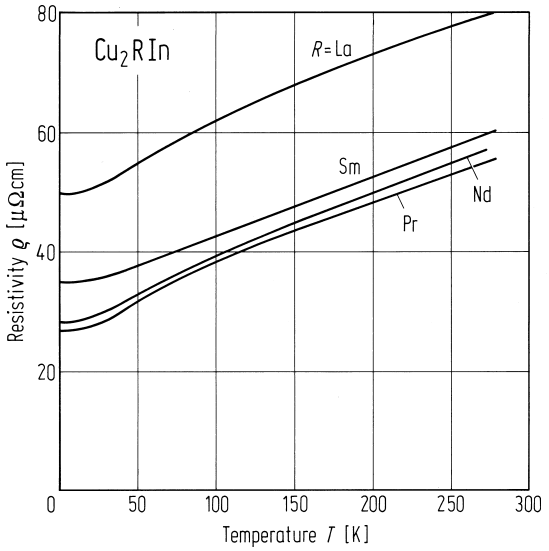

Fig. 274. Temperature dependence of the electrical resistivity of Cu_2RIn alloys with R = La, Sm, Nd, Pr. The current was applied along the [100] direction [91S1].

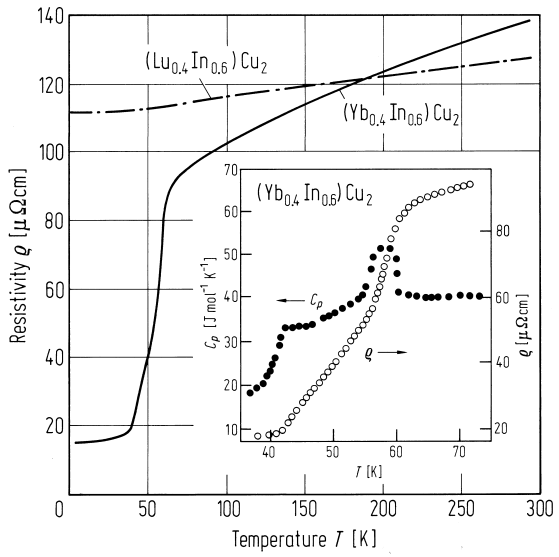

Fig. 275. Temperature dependence of the electrical resistivity of $Yb_{0.4}In_{0.6}Cu_2$ and $Lu_{0.4}In_{0.6}Cu_2$ from 4.2 K to room temperature. The inset shows details of the transition region with resistivity and specific heat data on an expanded scale [87F1].

X_2YZ X = 3d, 4d, Y = 4f

X = 1B: Cu, Ag
Y = 4A: La, Ce
Z = 3B: In

$Cu_xAg_{2-x}CeIn$

The resistivity of La compounds varies smoothly. With increasing Cu content x, the high temperature slope slightly decreases. The residual resistivity increases up to x = 1.8 and then remains nearly constant. With increasing x, the bulk resistivity of the Ce system increases. The magnetic resistivity

defined as the difference in the bulk resistivity of the Ce and La compounds exhibits a logarithmic decrease above 40 K. At lower temperatures, samples with x up to 1.95 order antiferromagnetically. The spin disorder term $\rho(T_N) - \rho(0)$ reveals a maximum near x = 1.5, then drops to a very small value near x = 2.

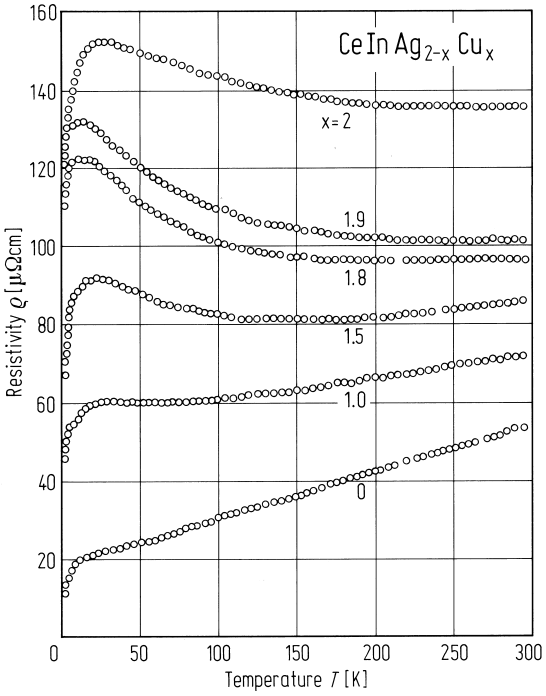

Fig. 276. Thermal dependence of the electrical resistivity of $CeInAg_{2-x}Cu_x$ alloys [87L1].

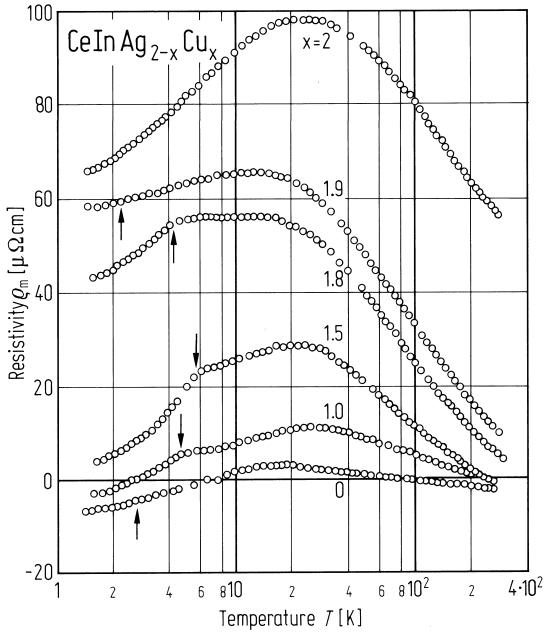

Fig. 277. Magnetic contribution to the electrical resistivity, ρ_m, of $CeInAg_{2-x}Cu_x$ alloys as a function of temperature [87L1].

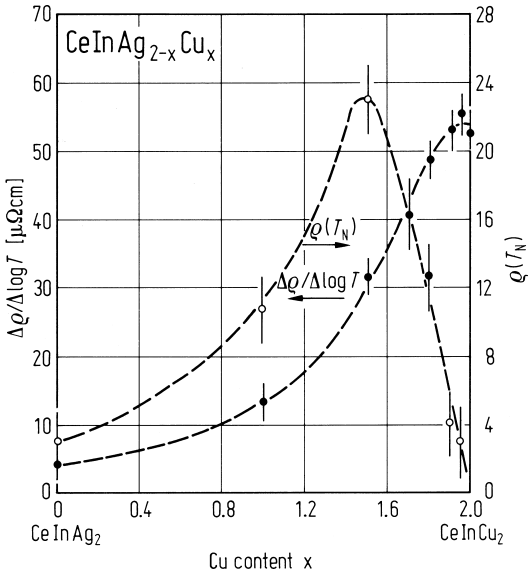

Fig. 278. Spin disorder resistivity at the Néel temperature and high temperature slope of the magnetic contribution to the electrical resistivity [87L1].

Ag_2YIn

The compounds containing Ce and Gd order antiferromagnetically below 2.7 K and 10 K, respectively. The absence of magnetic order in the Pr compound was confirmed down to 2 K.

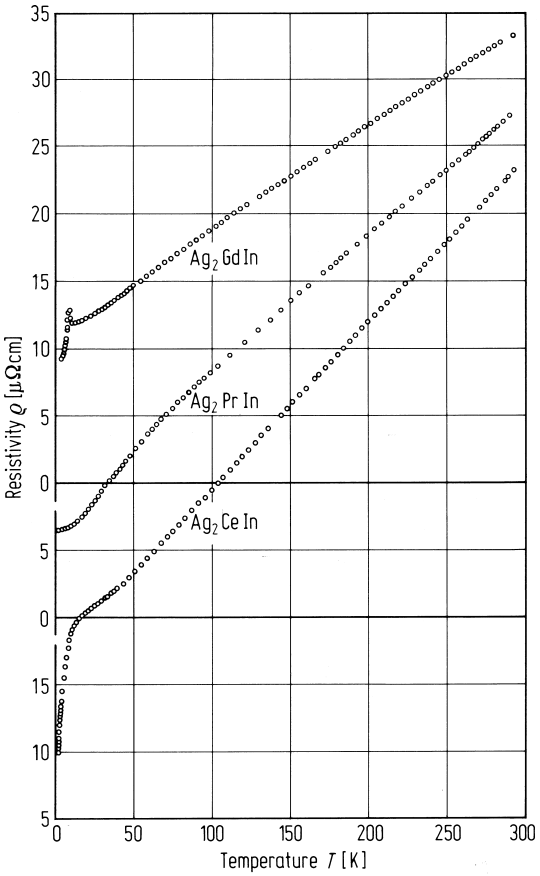

Fig. 279. Thermal variation of the electrical resistivities of Ag_2CeIn, Ag_2PrIn and Ag_2GdIn [84G1].

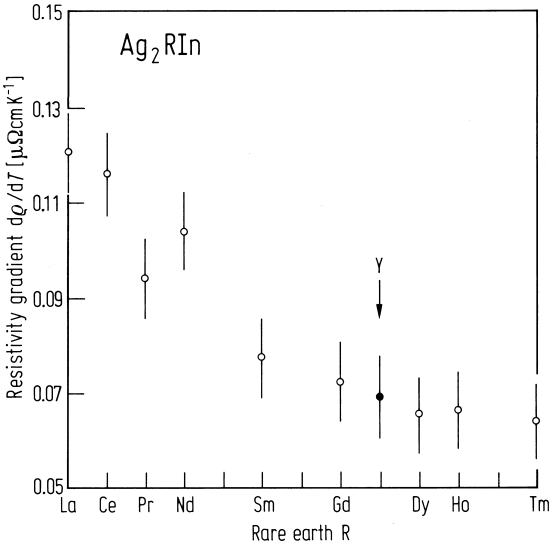

Fig. 280. A plot of the gradient of the resistivity observed between 200 and 300 K for compounds in the Ag_2RIn series [84G1].

X = 1B: Ag
Y = 4A: Gd, Tb, Dy
Z = 3B: In

$Ag_{1-x}YIn_x$

The compounds which form with the B2 structure order magnetically for certain values of x. The Gd compound is antiferromagnetic for $0 \le x \le 0.2$ and ferromagnetic for $0.2 \le x \le 0.5$. The Tb and Dy compounds are antiferromagnetic with T_N taking a minimum around x = 0.3 in both systems.

The magnetic interactions in these compounds are believed to be some indirect coupling such as the RKKY mechanism. Thus the pressure dependence of the Curie and Néel temperatures in $GdAg_{1-x}In_x$ compounds has been investigated. In hydrostatic pressures up to 6 kbar the Curie temperature shifted to higher values, but there was no change in the Néel temperature [78Y1].

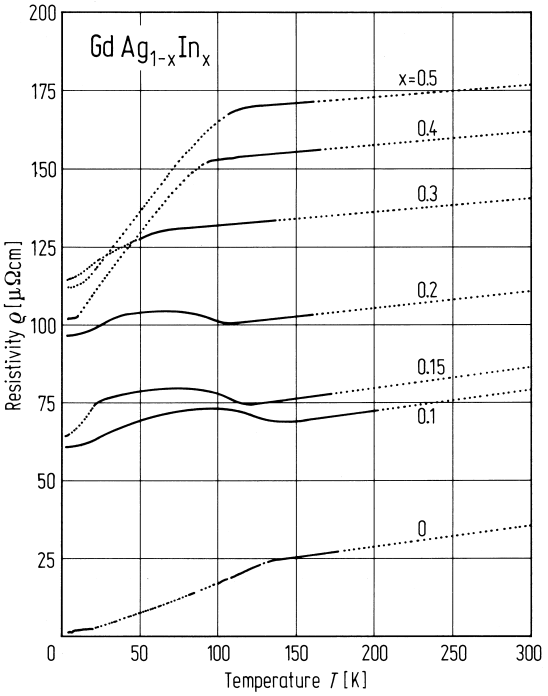

Fig. 281. Temperature dependence of the electrical resistivity for $GdAg_{1-x}In_x$ compounds [80Y1].

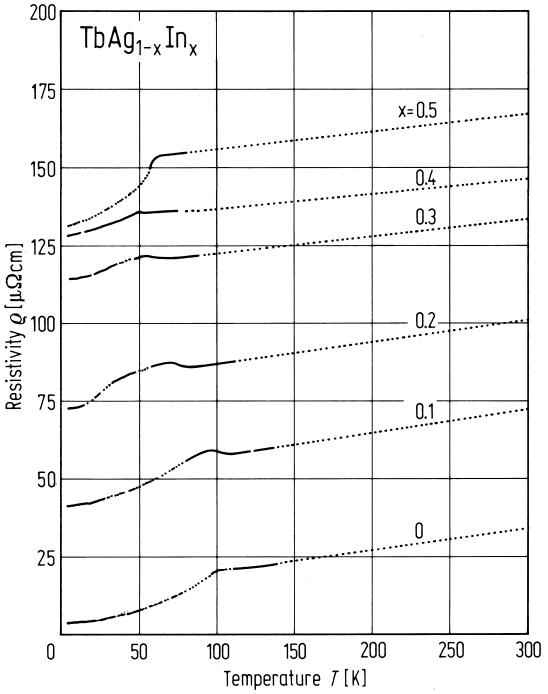

Fig. 282. Temperature dependence of the electrical resistivity for $TbAg_{1-x}In_x$ compounds [80Y1].

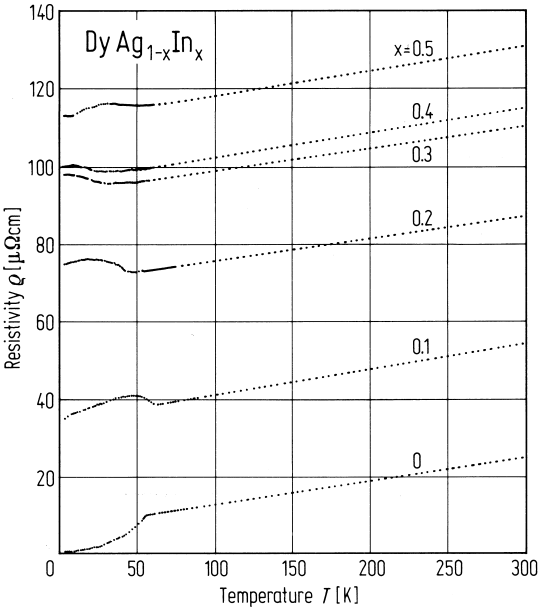

Fig. 283. Temperature dependence of the electrical resistivity for $DyAg_{1-x}In_x$ compounds [80Y1].

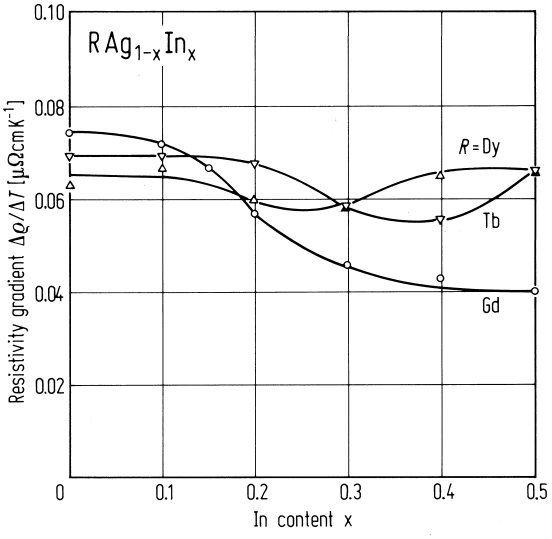

Fig. 284. A plot of $\Delta\rho/\Delta T$ against x for $RAg_{1-x}In_x$ compounds in the paramagnetic region [80Y1].

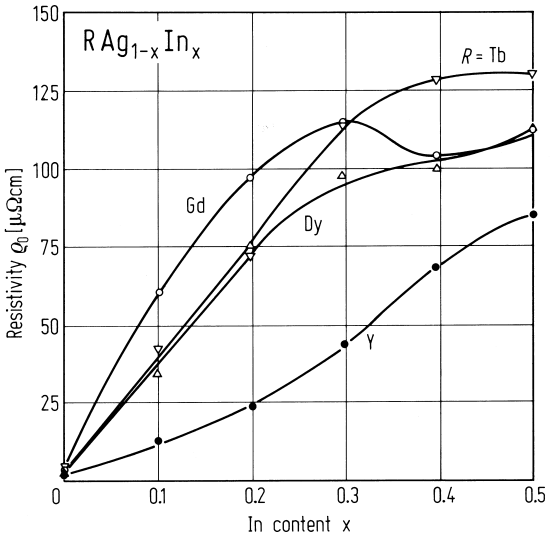

Fig. 285. A plot of residual resistivity ρ_0 against x for $RAg_{1-x}In_x$ compounds [80Y1].

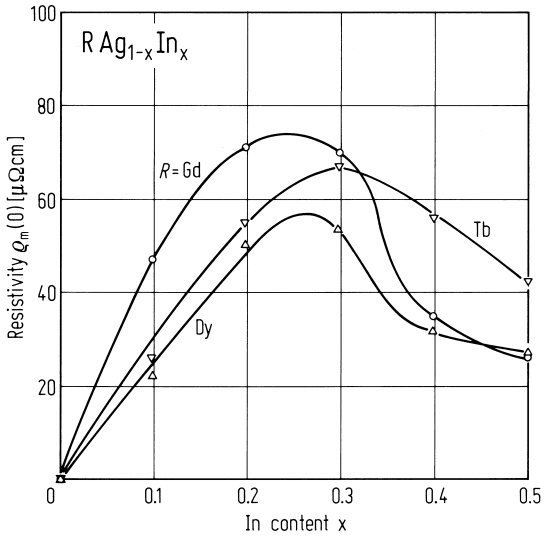

Fig. 286. A plot of the spin disorder scattering at 0 K $\rho_m(0)$ vs. x for $RAg_{1-x}In_x$ compounds [80Y1].

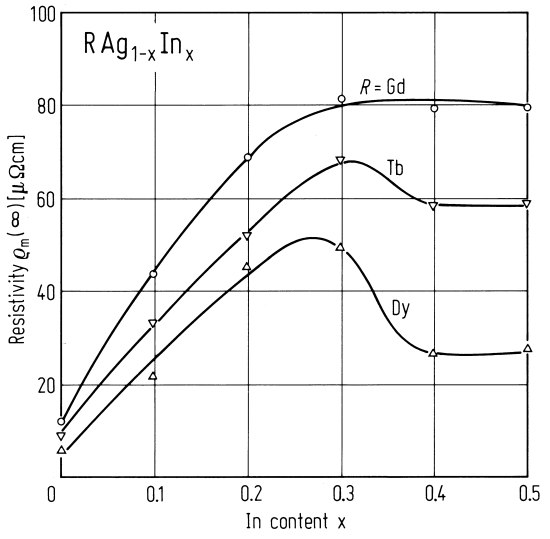

Fig. 287. A plot of the spin disorder scattering $\rho_m(\infty)$ vs. x for R Ag_{1-x} In_x compounds [80Y1].

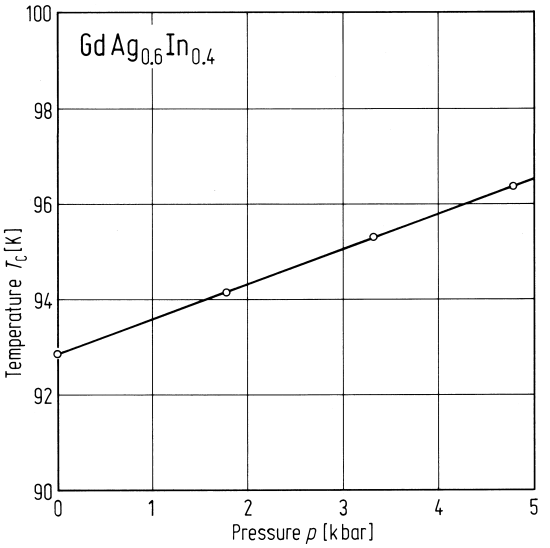

Fig. 288. Pressure dependence of T_C in $GdAg_{1-x}In_x$ for x = 0.4 [78Y1].

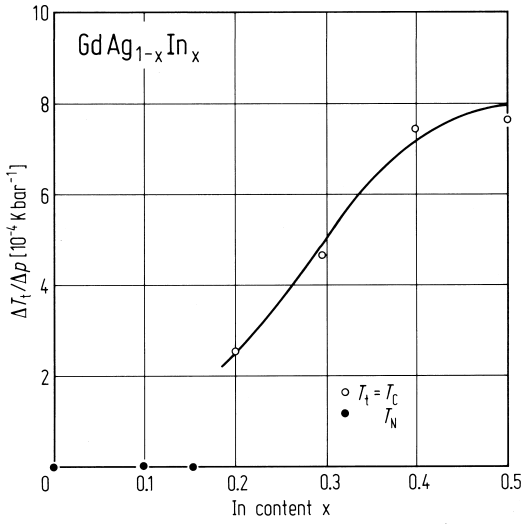

Fig. 289. A plot of $\Delta T_N/\Delta\rho$ and $\Delta T_C/\Delta\rho$ against x for $GdAg_{1-x}In_x$ compounds [78Y1].

Ni_2USn

To date, the only Heusler alloy which forms with an actinide element is Ni_2USn. However, around 200 K the system transforms to a structure of lower symmetry.

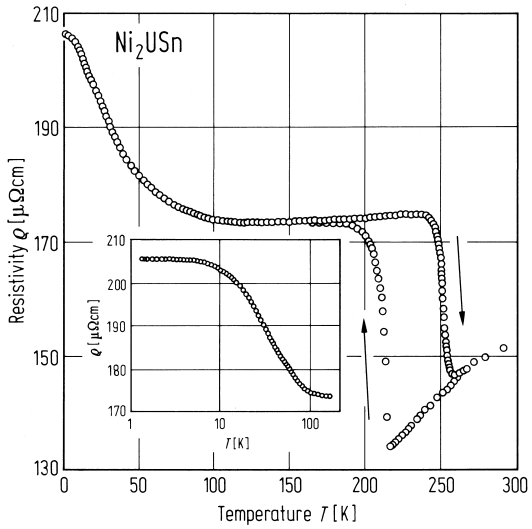

Fig. 290. Electrical resistivity vs. temperature of Ni_2USn indicating a phase transition around 200 K [90E1].

$C1_b$ compounds

XYZ X = 3d, 4d, Y = 3d

X = 8A: Co, Ni, Pd; 1B: Cu, Au
Y = 7A: Mn
Z = 4B: Sn; 5B: Sb

Interest in the $C1_b$ compounds has focused on the prediction that some should exhibit unusual electronic properties. The majority-spin electrons are metallic, whereas the minority-spin electrons are semiconducting [83D1]. Resistivity measurements have been made on a series of $C1_b$ compounds

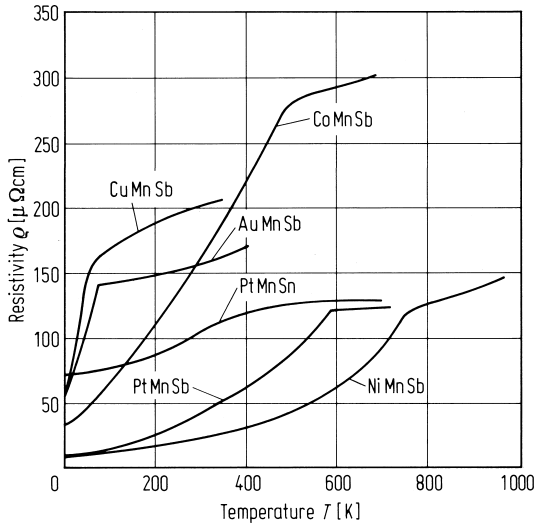

Fig. 291. Electrical resistivity ρ as a function of temperature for several $C1_b$ compounds [87O3].

over the temperature range 4…800 K. At low temperatures the resistivity of ferromagnets usually has a term proportional to T^2, due to spinflip scattering. However, this spinflip scattering is not possible in a half metallic-ferromagnet, because there are no states with the opposite spin orientation at the Fermi level at low temperatures. Neither NiMnSb nor PtMnSb exhibits a T^2 dependence in the low temperature resistivity.

1.5.5.6.2 Galvanomagnetic properties

X_2YZ X = 3d, Y = 3d

X = 8A: Ni
Y = 7A: Mn
Z = 3B: In; 4B: Sn; 5B: Sb

Ni_2MnZ

The galvanomagnetic properties have been investigated in order to quantify the effects of changing the electron concentration. Systematic effects are observed as the Fermi level is shifted, which have been interpreted using a delocalised description of the electron transport effects.

The transverse magneto-resistance of the three compounds containing In, Sn or Sb is similar to and typical for a ferromagnet. The field dependence of the Hall resistivity $\rho_{21}(B)$ has two parts: one saturating below ≈ 1 T and another that varies linearly with field. The former is the anomalous Hall effect (AHE) which is prominent in ferromagnets, exhibiting a bend in its field dependence. The anomalous Hall angle used to distinguish the microscopic scattering mechanism at an M site is defined by:

$$\theta_E = \theta_\hbar(T) = \left[\frac{\Delta\rho_{21}(T)}{\rho_0(T)}\right]\left(1/M_s^1\right) \tag{65}$$

where

$$M_s^1(T) = M_s(T)/M_s(4.2\text{K}) \tag{66}$$

The ordinary Hall coefficient R_0 is estimated from the gradient of $\rho_{21}(B)$ above saturation and at 4.2 K where complications from phonon scattering are minimised.